(Dis)Similarities of adsorption of diverse functional groups over alumina and hematite depending on the surface state

Sarah Blanck, Carles Martì, Sophie Loehlé, Stephan N. Steinmann, Carine Michel

(Dis)Similarities of adsorption of diverse functional groups over alumina and hematite depending on the surface state

Sarah Blanck,[1,2] Carles Martì,[1] Sophie Loehlé,[2] Stephan N. Steinmann,[1] Carine Michel[1,*]

1. Univ Lyon, Ens de Lyon, CNRS UMR 5182, Université Claude Bernard Lyon 1, Laboratoire de Chimie, F69342, Lyon, France
2. Total Marketing & Services, Chemin du Canal – BP 22, 69360, Solaize, France

*carine.michel@ens-lyon.fr

Abstract

To accelerate the conversion to more sustainable lubricants, there is a need for an improved understanding of the adsorption at the solid/liquid interface. As a first step, the DFT computed adsorption energies can be used to screen the ability of additives to cover a surface. Analogously to what has been found in catalysis with the universal scaling relations, we investigate here if a general universal ranking of additives can be found, independently of the surface considered. We divided our set of 25 diverse representative molecules into aprotic and protic molecules. We compared their adsorption over alumina and hematite, which are models of surface oxidized aluminum and steel, respectively. The adsorption energy ranking of our set is not strongly affected by alumina hydration. In contrast, adsorption on hematite is more strongly affected by hydration since all exposed Fe Lewis acid sites are converted into hydroxylated Brønsted basic sites. However, the ranking obtained on hydrated hematite is close to the one obtained on dry alumina, paving the road to a fast screening of additives. In our library, protic molecules are more strongly adsorbed than non-protic molecules. In particular, methyl and dimethyl phosphates are the most strongly adsorbed ones, followed by N-methyldiethanolamine, succinimide and ethanoic acid. Additives combining these functional groups are expected to strongly adsorb at the solid/liquid interface and, therefore, likely to be relevant components of lubricant formulations.

Introduction

Modeling the adsorption at the solid-liquid interface is central to challenges that emerged recently with the quest for a more sustainable chemical industry, from impact of the biproducts soil pollution[1], biomass valorisation[2] and electrocatalysis[3] to improved industrials additives[4] such as corrosion and fouling inhibitors. The modeling strategy differs strongly from one field of application to the next, and a cross-pollination could be fruitful. When a chemical reaction is clearly targeted as in heterogeneous (electro)-catalysis, computing adsorption energies at the Density Functional Theory (DFT) level is the work-horse, sometimes supplemented with more or less advanced solvent models.[5–7] In this field, a great attention is also given to the surface state and its impact. While the surface modification by water for instance can be critical to describe the reactivity in specific cases[8], it appears that adsorption of small typical fragments follow universal scaling relations on bare surfaces[9–12], making the adsorption ranking conserved from one material to the next. When it comes to lubricant additives, the modeling of adsorption at the solid-liquid interface relies mainly on molecular mechanics driven molecular dynamics, where non-bonding force fields are used to investigate the structural arrangement of the additives at the interface between the treated surface and the base oil.[13–16] The possible strong, and eventually dissociative, chemisorption of the additive polar head cannot be taken into account through this approach and the relative strength of adsorption of one additive to the next is thus rarely determined. However, adsorption has been identified as an important parameter of the lubricant's performances. In particular, the adsorption energy can influence the lubricant's wettability[13,14] as well as its tribological properties[17,18]. Thus, just like in heterogeneous catalysis[19], DFT computations are ideally suited to assess adsorption free energies of additives under controlled conditions[20]. Phosphates and carboxylic acids were found to be the most strongly adsorbed on dry alumina, and thus more likely to yield to improved lubrication. However, for practical considerations, both for theory and for experiment, it is essential to know if screening of additive functional groups on a dry surface model is transferable to other hydration states and even to other materials. Indeed, in analogy to the popular use of linear scaling relationships over transition metal surfaces[21,22], it would be highly beneficial if the screening of additives could be extended from one surface to the next at minimal computational and human effort. A fast and efficient prediction of promising new additives is expected to accelerate the development of new lubricants able to satisfy ever stricter regulations not only regarding the composition[23] but also the emission of pollutants[24], while moving towards greener formulations.

Aluminum and steel are commonly used together with lubricants in metal working and in internal combustion engines. Both aluminum and steel surfaces oxidize when exposed to air. Thus, we will use

their respective oxides alumina and hematite to model the surfaces of these metals, in their dried and hydrated surface states. We aim at providing a comprehensive study of the adsorption behavior on these surfaces of a library of 25 diverse functional groups, characteristic for lubricant additives. This library might, subsequently, be used to establish group-additivity models[25–27] for complex multi-functional molecules for high-throughput screening, or the data might be complemented by solvation free energies in various solvents and base-oils to assess the influence of the liquid phase on the established trends[20]. Since many of the functional groups we selected are also commonly found in chemicals relevant for catalytic transformations, the extension to the hydrated surfaces of alumina and hematite is all the more relevant in view of gaining insights of the behavior of various functional groups at the solid/water interface as exposed under (photo-) catalytic conditions.[28,29]

The next section describes the computational details, the adopted surface models and presents the chosen molecules to probe the adsorption behavior. Section 3 starts by presenting the trends of adsorption energies on the bare surfaces, before comparing them to the situation of the hydrated surfaces. All along, the similarities and differences between hematite and alumina will be highlighted.

Materials and methods

1. Computational details

All calculations were performed at the DFT level as implemented in CP2K[30]. A hybrid gaussian and plane waves (GPW) basis set[31,32] was used, with a 400 Ry energy cutoff for plane waves. The Molopt double-ζ basis set was used to describe the valence electrons and the core electrons were treated with the Goedecker, Teter and Hutter (GTH) pseudopotentials[33–36]. The Perdew, Burke and Ernzerhof (PBE)[37] functional was employed to compute the exchange and correlation energies, along with the DFT-D3 the dispersion correction of Grimme et al. including C9 terms[38,39]. The use of the chosen functional is supported by a benchmark study of water over alumina where both adsorption energy and structural parameters were found to be in agreement with both MP2 methods and hybrid functionals like B3LYP and HSE06[40]. Furthermore, the functional have been extensively used in the community when computing adsorption energies(PBE, PW91)[41–44].

The energies were converged to 10^{-7} Ha during the self-consistent field (SCF) process and the geometries were optimized to forces below 4.5×10^{-4} Ha/bohr. All calculations were performed at the Γ-point of the Brillouin zone.

The different surfaces used in this study (alumina, hydrated alumina, hematite, and hydrated hematite) are modeled by periodic slabs. For each surface, the bottom layers of the slab are kept frozen to mimic the bulk material, whereas the top layers are free to adapt to the adsorption of a molecule. A 20 Å vacuum layer has been set between two periodically repeated slabs to minimize interactions between them.

The adsorption energy of a molecule on a given surface is calculated respect its gas phase and is defined as:

$$E_{ads} = E_{molecule@surface} - (E_{surface} + E_{molecule})$$

where all energies are calculated at vacuum. The solvation of the studied molecules in the industrial oil can be neglected compared with the strength of adsorption.[20]

For hematite, which is an antiferromagnetic oxide[45,46], we applied the DFT+U method[47] to account for the strong electronic correlation of Fe localized 3d electrons. This method, relying on the combination of DFT with a Hubbard-Hamiltonian[48] in order to explicitly consider the Coulombic repulsion, has shown to be useful to achieve agreement with experimental values of different properties of hematite[49–52] and it is widely used in theoretical studies of adsorption of different species over hematite[53–56]. The DFT+U contribution calculation used here is based on Mulliken gross orbital population (GOP). The U-J parameter was converged so that the band gap energy of the bulk reproduces the experimental one (i.e. 2.2 eV[57]), which resulted in a value of 5 eV according to ref [46].

2. γ-alumina

γ-alumina is one of the main alumina oxides investigated, together with α-alumina. It is a commonly used material, especially as a support in heterogeneous catalysis but also as a model for the surface oxides encountered in metal working and lubrication[20,58,59]. γ-alumina mainly exposes three surface terminations: the (100), the (110) and the (111) facets. Here, like in our previous study[20], we choose to work on the (100) facet, which has the lowest surface energy[60] and is, therefore, likely to be the most abundant one.

As shown on Figure 1a, the (100) alumina p(1x1) unit cell exposes four aluminum atoms, all of them being coordinated to five oxygen atoms. Among these aluminum atoms, the ones labeled Al_{Vb} and $Al_{Vb'}$ are equivalent. Al_{Va} is the most reactive one[20], due to its higher acidity[61]. This surface also exposes three non-equivalent oxygen atoms, coordinated to three (O_{3a}, $O_{3a'}$, O_{3b} and $O_{3b'}$) or four aluminum atoms (O_4 and $O_{4'}$).

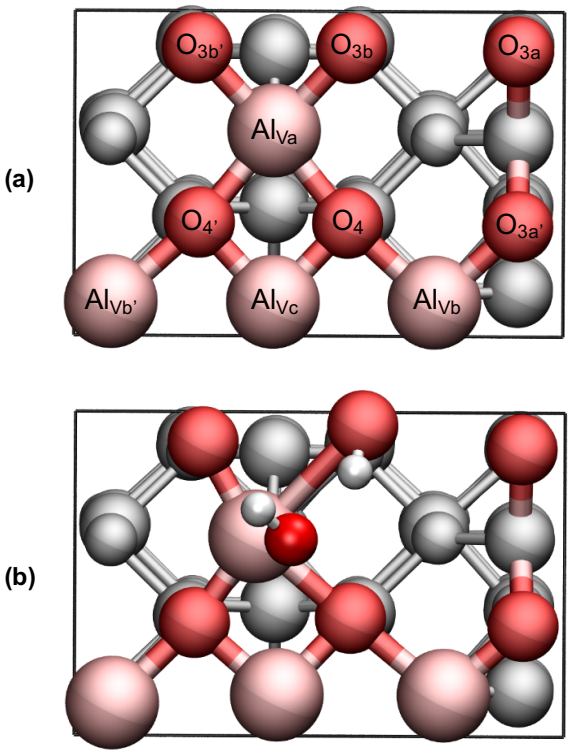

Figure 1: Top view of the p(1x1) unit cell of (a) alumina and (b) hydrated alumina. Only the exposed atoms of the surface and the dissociated water molecule are colored (oxygen atoms in red, aluminum atoms in pink and hydrogen atoms in white). A supercell was used to model the adsorption of the studied molecules.

Under ambient conditions, alumina is naturally hydrated due to the presence of water in the air. A varying number of water molecules can be adsorbed on the surface depending on the temperature[60], but only the water molecule adsorbed on Al_{Va} is dissociated, protonating O_{3b}.

As the non-dissociated adsorbed water molecules can be easily displaced by the adsorption of other molecules, only the dissociated water molecule was considered on the hydrated alumina surface (Figure 1b) to compute the adsorption of the studied molecules from the gas phase to the surface.

For both alumina and hydrated alumina surfaces, we used a p(2x2) unit cell, with a thickness of 15 Å ($Al_{128}O_{192}$). These slabs present a total number of 14 atomic layers, 8 of which were frozen during the geometry optimizations to mimic the bulk structure of the material. The cell matrix used (a=(11.074, 0, 0) b=(0, 16.714, 0) c=(0, 0, 35.0) Å) resulted in distances between periodic images of studied adsorbed molecules higher than 5.3 Å.

3. Hematite

Hematite, α-Fe_2O_3, is the most abundant iron oxide on earth[49] and is of interest in a wide range of applications including energy storage[52,62] and catalysis[52,63,64]. In this paper, we chose the representative hematite (0001) surface as a model for the oxidized steel surface, in agreement with several previous studies[65–67].

The p(1x1) unit cell of this facet (Figure 2a) exposes three equivalent tri-coordinated oxygen atoms and three iron atoms, two of them being slightly below the surface and coordinated to six oxygen atom (labeled Fe_{VI}), and the third one being coordinated to three oxygen atoms (Fe_{III}).

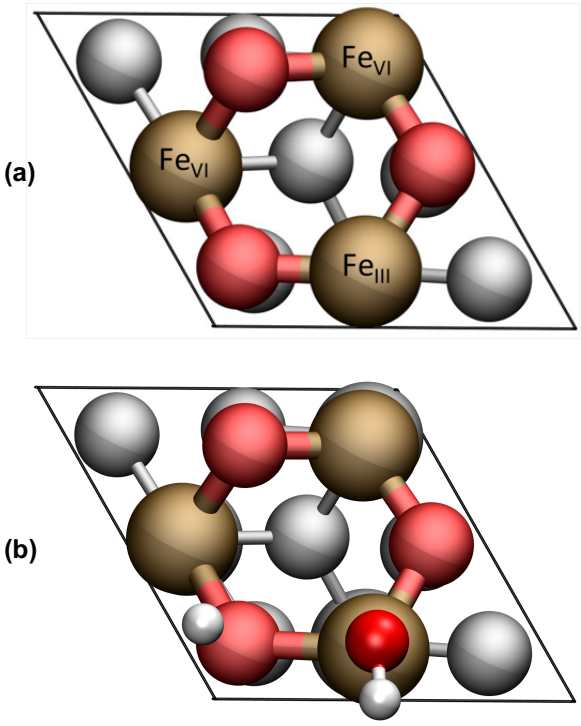

Figure 2: Top view of the p(1x1) unit cell of (a) hematite and (b) hydrated hematite. Only the exposed atoms of the surface and the dissociated water molecule are colored (oxygen atoms in red, iron atoms in brown and hydrogen atoms in white). A supercell was used to model the adsorption of the studied molecules.

Like alumina, hematite can be hydrated by the relative humidity under ambient conditions. A certain quantity of water molecules will thus be adsorbed on the surface depending on the temperature. Souvi et al.[67] have shown that at 300 K, hematite presents two adsorbed water molecules per unit cell. Only one water molecule is dissociated. We choose to keep only the dissociated water molecule on the hydrated hematite surface, leading to the structure shown in Figure 2b, with one hydroxyl group adsorbed on the tri-coordinated iron atom Fe_{III} and one hydrogen atom bonded to an oxygen atom of the surface.

The hematite and hydrated hematite surfaces used for DFT calculations are modeled by a p(3x3) unit cell, having a thickness of 6 Å ($Fe_{54}O_{81}$), i.e. nine atomic planes, four of which were kept frozen during the simulations. This surface was chosen thinner than the one of alumina due to the higher computational costs of the calculations involving hematite which result from its magnetization. The cell matrix used (a=(15.3822, 0, 0) b=(-7.6911, 13.32138, 0) c=(0, 0, 27.0) Å) resulted in distances between periodic images of studied adsorbed molecules higher than 8.8 Å.

4. Studied molecules

A diverse library of molecule is studied herein, covering most common chemical functional groups. Even though they can be of interest for various applications[64,68], the molecules have been chosen with a special attention to be representative of the typical additives used in various industrial lubricant applications such as thermal engine, metal working, gear box… Fatty ethoxylated amines and fatty acid derivatives are often used as organic friction modifiers[4,69,70] whereas fatty amines are good anti-corrosion additives[4]. Phosphates are presenting good extreme-pressure properties, but can also be used as detergents, just like fatty acids.[4] Generally speaking, multi-functional additives are commonly used. Hence, to emphasize the impact of each functional group, additives have been simplified to mono-functional molecules. The adsorption of multi-functional additives can easily be derived using a group additivity approach that has already been proven efficient in heterogeneous catalysis[25–27]. In addition, alkyl chains enabling solubility and/or formation of layer(s) have been removed to focus on the polar head group and its interaction with the substrate.

As some molecules can be found in different additive categories, we decided to split the 25 studied molecules into two categories depending on their chemical properties: protic and aprotic molecules (Table 1 and Table 2).

Table 1: Protic molecules

Molecule number	Name of the molecule	Structure of the molecule
1	Water	
2	Ammonia	

3	Methylamine	
4	Dimethylamine	
5	N-methyldiethanolamine	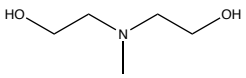
6	Methanol	
7	Methanethiol	
8	Ethanoic acid	
9	Triazole	
10	Pyrazole	
11	Succinimide	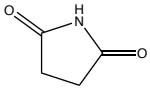
12	N-methylacetamide	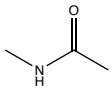
13	Phenol	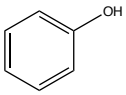
14	Methylphosphate	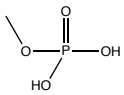
15	Dimethylphosphate	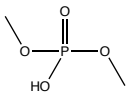

Table 2: Aprotic molecules

Molecule number	Name of the molecule	Structure of the molecule

16	Dimethylether	
17	Propanone	
18	Methyl ethanoate	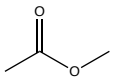
19	Dimethylsulfide	
20	Trimethylamine	
21	N,N-dimethylacetamide	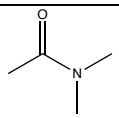
22	1-methyltriazole	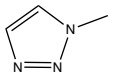
23	Acetonitrile	
24	Benzene	
25	Trimethylphosphate	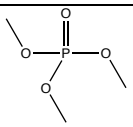

An extensive and systematic search for the best adsorption structure has been performed for each molecule. Different gas phase conformers were generated in order to find the most stable one. Using this conformer, a great number of structures was generated to sample the molecule-surface chemical space. The different potential adsorption centers of the molecule (see for instance molecule **5**), the various possible adsorption sites on the surface, as well as different orientations of the molecule over the surface were taken into account. The possibility of proton dissociation has also been systematically considered for protic molecules.

Results and discussion

1. Effect of the type of surface

Alumina and hematite are both non-conducting oxides and present similarities in terms of reactivity properties.[71,72] Nevertheless, some important differences exist between the two materials. Firstly, hematite is antiferromagnetic whereas alumina is not. Moreover, the distance between adsorption sites is lower on alumina (between 2.6 and 2.9 Å) than on hematite (5.1 Å), thus facilitating bidentate adsorption modes on the former. Furthermore, the investigated alumina surface exposes three Al atoms with varying Lewis acid strengths. This could induce a significant difference concerning the adsorption mode and energy of the various molecules, and, therefore, in their ranking in terms of adsorption energy from one surface to the other.

The comparison of the adsorption energies obtained for the set of studied molecules on the (100) γ-alumina surface and on the (0001) hematite surface is given on Figure 3. For protic as well as for aprotic molecules, the points obtained are above the diagonal of the graph, indicating that hematite is more reactive than alumina for all the studied molecules, leading to more exothermic adsorption on hematite. Importantly, the points obtained are nonetheless located around the same line, demonstrating that the ranking of the different functional groups is nearly equivalent on the two surfaces: for both alumina and hematite, methylphosphate and dimethylphosphate (**14** and **15** respectively) are the most adsorbed molecules. On the other hand, benzene (**24**) and acetonitrile (**23**) are the least adsorbed ones.

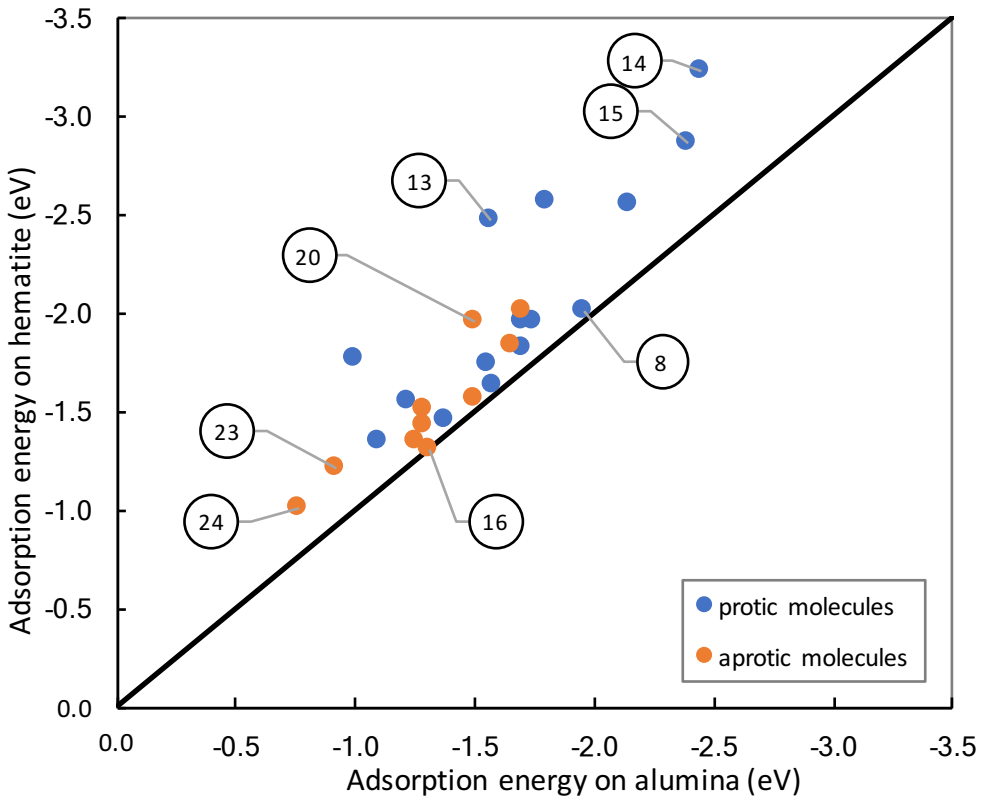

Figure 3: Comparison of adsorption energies obtained for the different molecules studied on alumina and hematite. Blue points refer to protic molecules (Table 1) and orange points to aprotic molecules (Table 2). The corresponding molecule numbers, as listed in Table 1 and Table 2, are given for some selected points.

Despite the overall similarity of the relative adsorption energies, a limited number of points deviate significantly from the linear trend. In particular, molecule **13**, corresponding to phenol, is the one presenting the greatest difference (0.9 eV) in adsorption energy between the two surfaces. Phenol is dissociated on both surfaces (Figure 4). However, while the proton is 2.65 Å away from the phenol oxygen atom on hematite, it is only at a distance of 1.65 Å on alumina, indicating that the proton is shared between the oxide and the adsorbate, in agreement with the overall lower reactivity of alumina compared to hematite.

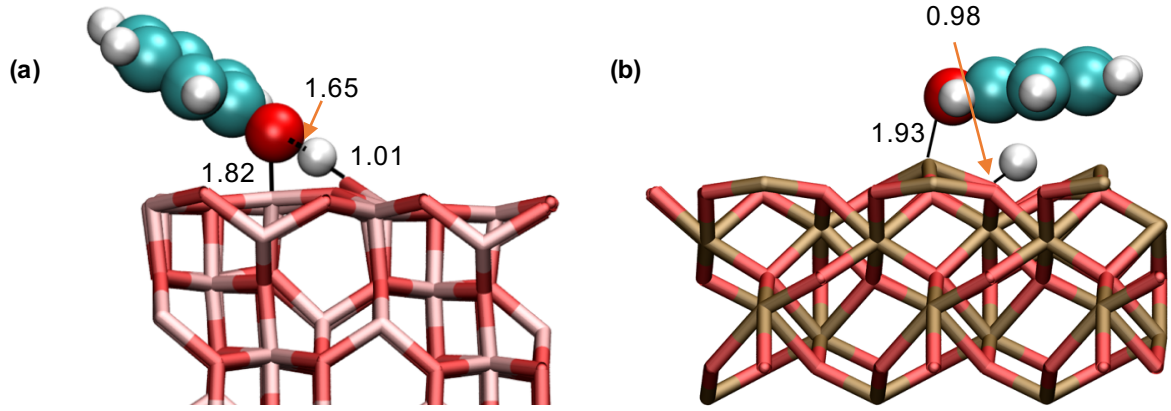

Figure 4: Phenol adsorption on (a) alumina and (b) hematite. Bonds between the molecule and the surface are indicated by continuous lines and hydrogen bonds by dashed lines. Typical bond distances are given in Angstroms.

Ethanoic acid (**8**) has, on the contrary, very similar adsorption energies on hematite and on alumina. This can be explained by the fact that its adsorption on alumina adopts a bidentate mode, which is impossible on hematite due to the too large distance (5.1 Å) between two adsorption sites. Thus, the bidentate adsorption on alumina is compensating the stronger reactivity of hematite. Hence, despite varying adsorption modes (shown in Figure S3), carboxylic acids adsorb equally strongly on both surfaces.

The analysis is slightly more complex for aprotic molecules. From the structural point of view, dimethylether (**16**) and trimethylamine (**20**) are adsorbed in an analogous manner, which is not affected by the nature of the surface (see Figure S4 and S5 respectively): the oxygen atom of dimethylether and the nitrogen atom of trimethylamine are adsorbed on an aluminum atom or an iron atom. However, the adsorption energies are affected in a contrasted manner by the surface nature. Dimethylether is adsorbed on both surfaces with the same adsorption energy (-1.31 eV), whereas trimethylamine is more strongly adsorbed on hematite than on alumina by 0.45 eV. In other words, the higher reactivity of hematite compared to alumina, which can easily explain the difference in adsorption energies obtained for trimethylamine, is not reflected in the adsorption energies values obtained for dimethylether. This might be related to the difference in hardness of the Lewis acids (Al^{3+}>Fe^{3+}) and bases (OR_2> NR_3)[73,74].

In summary, even if the Fe_{III} site of hematite is overall more reactive than the Al_{Va} site of alumina, the differences in adsorption strength observed between these two surfaces are limited and can be rationalized. In particular, adsorption on hematite can be weakened compared to alumina due to the distance between the Lewis-acid sites on the surface (5 Å vs less than 3 Å on alumina), which tunes the adsorption of multidentate molecules. For protic molecules, which dissociate on both surfaces, the

geometrical constraints of the resulting surface OH group that can lead to hydrogen bonds with the adsorbate, modulate somewhat the relative adsorption energies on the two surfaces.

2. Effect of the hydration of the surface

Under ambient conditions, both surfaces are at least partially hydrated, with water molecules dissociating on the bare surfaces to yield two hydroxyl groups per dissociated water molecule. Compared to the Lewis-acidity of the bare surfaces, these hydroxyls might radically change the adsorption behavior, including the adsorption mode, of various functional groups.

1. Alumina and hydrated alumina

The Al_{Va} aluminum atom is the most reactive one on the (100) γ-alumina surface. Thus, when considering the adsorption of molecules on the non-hydrated alumina surface, most molecules are preferentially binding with this site[20]. On the hydrated alumina surface, this Al_{va} site is, however, already occupied by the dissociated water molecule. Therefore, the adsorption mode of the adsorbates has to involve other, less favorable, adsorption sites. But the presence of the dissociated water molecule allows also the formation of stabilizing hydrogen bonds between the molecule and the surface. Hence, it is not obvious which one of the two effects (destabilizing or stabilizing) is overall dominant or if the balance between the two varies a lot with the nature of functional group of the adsorbate.

The adsorption of N-methyldiethanolamine **5** is a good illustration of the various rearrangements that may be initiated by the presence of the dissociated water molecule on the hydrated surface (Figure 5). On the bare surface (Figure 5a), only one oxygen atom of the molecule binds the surface. In contrast, on the hydrated surface (Figure 5b), the two oxygen atoms of the molecule are in close contact with the surface. Furthermore, the surface OH has deprotonated one of the hydroxyl groups of the molecule, leading to a non-dissociated water molecule adsorbed on the surface. This co-adsorbed state is stabilized by three hydrogen bonds, indicated by dotted lines. As a result, the adsorption energy of N-methyldiethanolamine is stronger on hydrated alumina than on the bare surface: -2.16 and -1.80 eV respectively (Figure 6, point **5**).

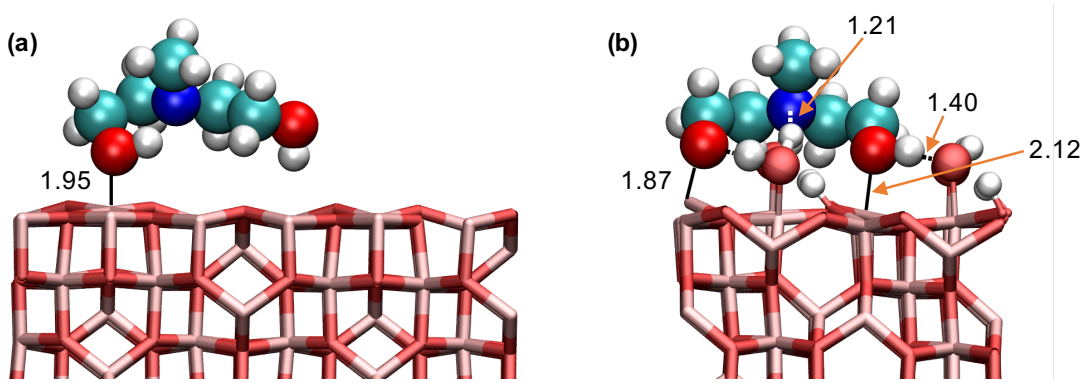

Figure 5: N-methyldiethanolamine adsorption on alumina (a) and hydrated alumina (b). Bonds between the molecule and the surface are indicated by continuous lines and hydrogen bonds by dashed lines. Typical bond distances are given in Angstroms.

However, the behavior of N-methyldiethanolamine is rather the exception than the rule, as evidenced by the parity plot for the entire library of adsorbates (Figure 6). In fact, the majority of points are situated close to the diagonal of the graph, with a slight tendency to being below, i.e., adsorption on hydrated alumina is, in general, only slightly less favorable than on the dry surface. Hence, the surface state of alumina does not influence the relative adsorption energies of various functional groups.

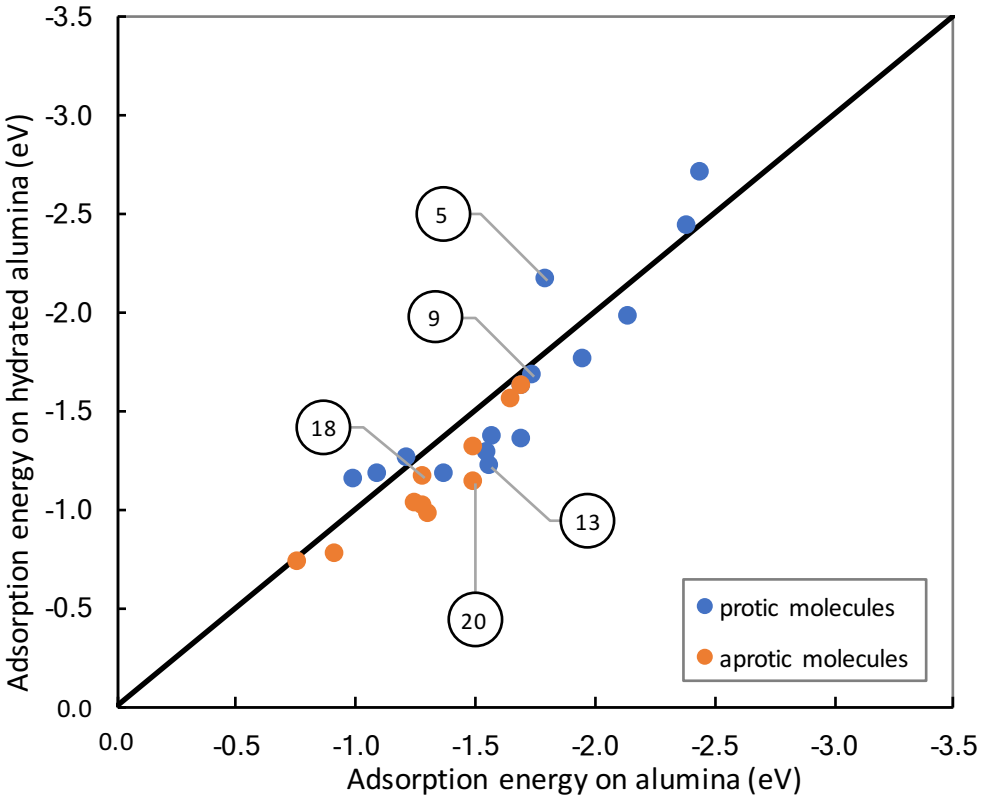

Figure 6: Comparison of adsorption energies obtained for the different molecules studied on alumina and hydrated alumina. Blue points refer to protic molecules (Table 1) and orange points to aprotic molecules (Table 2). The corresponding molecule numbers, as listed in Table 1 and Table 2, are given for some selected points.

Let us now analyze a few more points of Figure 6 to better understand the origin of the obtained similarity between the adsorption on the hydrated and the bare (100) γ-alumina surface.
Trimethylamine (**20**) is adsorbed in a similar way on both alumina surfaces: the nitrogen atom of the molecule is binding to an aluminum atom of the surface (Figure S6). But as the most reactive aluminum is already occupied by the dissociated water molecule on the hydrated alumina surface, the molecule is no longer adsorbed on Al_{Va} but on $Al_{Vb'}$. The fact that trimethylamine is adsorbed on a less reactive aluminum atom explains its weaker adsoption energy on the hydrated surface as it can be seen on Figure 6, where point **20** is clearly lying below the diagonal.

Similarly, phenol (**13**) is more strongly adsorbed on the non-hydrated surface due to the differences in Lewis acidity of the different aluminum sites. In addition, the molecule is dissociated on the non-hydrated surface, illustrating even qualitatively the stronger adsorption on this surface (see Figure S7).

For methyl ethanoate (**18**), the optimal adsorption structure on hydrated alumina is obtained with the molecule being physisorbed on the surface. The oxygen atom, which is adsorbed on the non-hydrated surface, is here linked by a hydrogen bond to a reconstructed water molecule. Apparently, hydrogen bonding to the adsorbate has increased the Brønsted basicity of the surface OH, so that it has recaptured the proton from the neighboring O_{3b} site. It turns out that in this case the two effects cancel each other, so that point **18** falls on the diagonal of Figure 6.

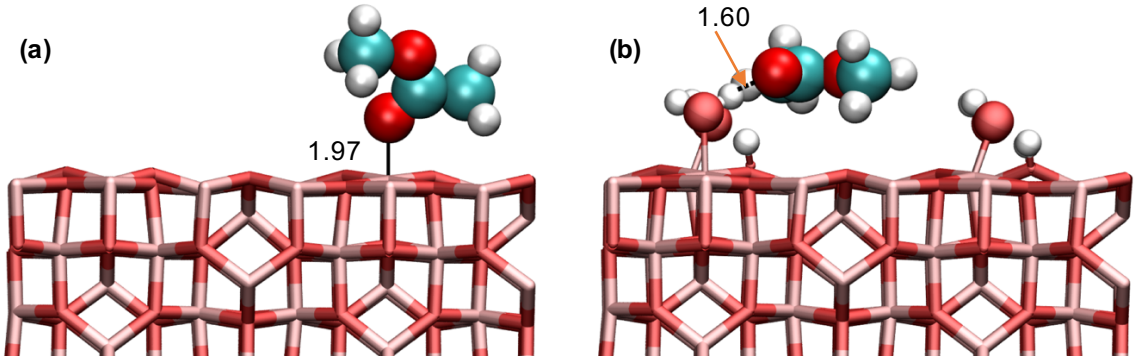

Figure 7: Methyl ethanoate adsorption on alumina (a) and hydrated alumina (b). Bonds between the molecule and the surface are indicated by continuous lines and hydrogen bonds by dashed lines. Typical bond distances are given in Angstroms.

Point **9**, corresponding to triazole, is also almost on the diagonal, meaning that the adsorption energies on alumina and hydrated alumina are similar. Nevertheless, the structures obtained on the two surfaces are very different (Figure 8). On bare alumina, the molecule is dissociated and two nitrogen atoms are binding to the surface, whereas on the hydrated surface only one nitrogen binds to the surface. In both cases, a hydrogen bond is present: between the dissociated hydrogen and one of the

nitrogen atoms of the triazole on bare alumina, and between the protic hydrogen of the molecule and a surface hydroxyl group on hydrated alumina. This example illustrates that the correlation of adsorption energies observed in Figure 6 hides the full complexity of the actual adsorption behavior.

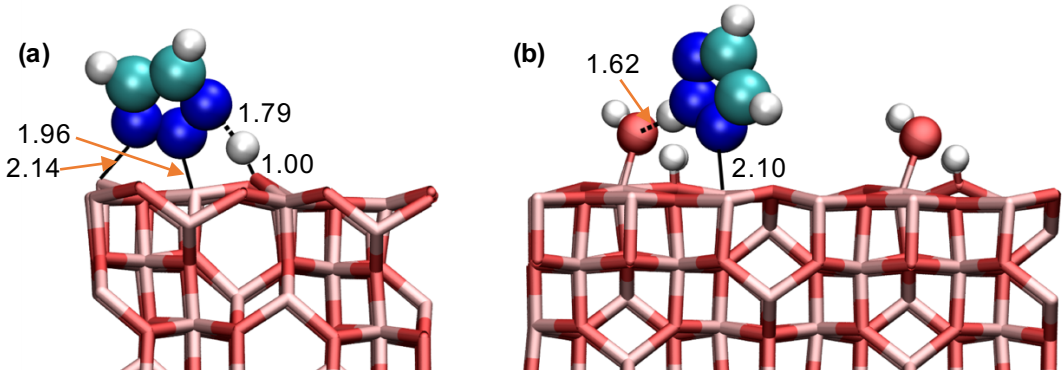

Figure 8: Triazole adsorption on alumina (a) and hydrated alumina (b). Bonds between the molecule and the surface are indicated by continuous lines and hydrogen bonds by dashed lines. Typical bond distances are given in Angstroms.

In summary, the adsorption modes differ substantially between bare and hydrated alumina due to a subtle interplay between the Lewis acidity of the available Al sites, the basicity of the surface OH and the possibility to form hydrogen bonds. Our results demonstrate, however, that the energetic impact of these variations nearly cancel out, so that the ranking of relative adsorption energies on the dry surface is largely valid for the hydrated one as well, facilitating the screening of more complex adsorbates.

2. Hematite and hydrated hematite

Unlike alumina, on the (0001) surface of hematite only the Fe_{III} atom is under-coordinated, leading to a single possible adsorption site. All chemisorbed molecules will, therefore, bind to this iron atom in one way or another. On hydrated hematite, however, the dissociated water molecule already occupies this adsorption site. Thus, the surface hydroxyl group could stabilize the adsorbed molecule by H bonding like on hydrated alumina, but on hematite, no other iron adsorption site is available for another functional group of the adsorbate. In absence of those strong Lewis acid sites, we can assume that the adsorption will be significantly weaker on the hydrated surface.

Figure 9 shows the comparison of the adsorption energies obtained on hematite and hydrated hematite. Most points are below the diagonal of the graph, indicating that the adsorption is, indeed, generally stronger on the bare hematite surface. The deviation from the diagonal is, furthermore, most important for protic molecules. Importantly, the extrema of the adsorption energies are conserved (benzene is the most weakly bound, while the two protic phosphates are most strongly adsorbed), but

the middle zone is squeezed into a rectangle, with a larger spread on the bare than on the hydrated surface (1.5 eV vs 1.0 eV).

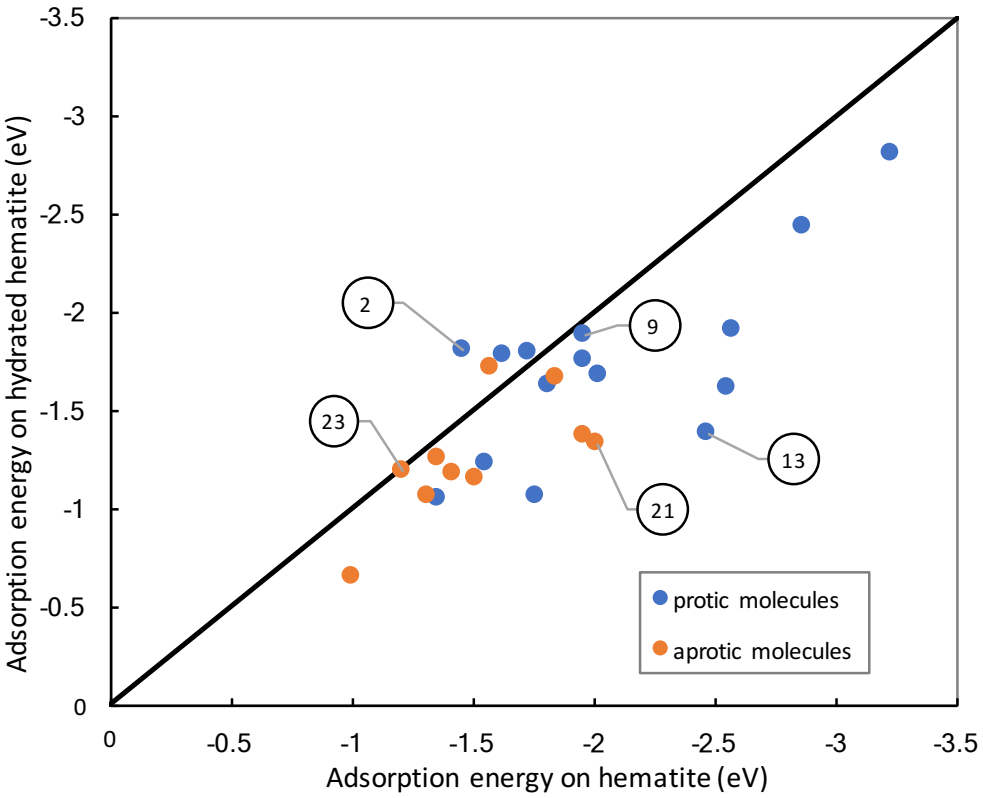

Figure 9: Comparison of adsorption energies obtained for the different molecules studied on hematite and hydrated hematite. Blue points refer to protic molecules (Table 1) and orange points to aprotic molecules (Table 2). The corresponding molecule numbers, as listed in Table 1 and Table 2, are given for some selected points.

Phenol (**13**) presents the largest difference in adsorption energy between the two hematite surfaces. For this molecule, the adsorption is more favorable on the non-hydrated than on the hydrated hematite by 1.12 eV. While phenol is strongly chemisorbed on the bare surface (with the O-H bond broken as shown Figure 4), this adsorption mode is no longer possible on the hydrated surface. Instead, phenol is only forming hydrogen bonds with the surface hydroxyls (see Figure S8). Unlike the case of methyl ethanoate on alumina, these hydrogen bonds are, however, not able to compensate the stronger chemisorption on bare hematite.

Ammonia (**2**) provides a counter example: even though NH_3 is only interacting with the hydrated surface through hydrogen bonds, its adsorption is more favorable on hydrated hematite than on the bare surface by 0.34 eV. Indeed, the symmetry and size of NH_3 is ideally fitting on the hydrated surface, achieving three hydrogen bonds with neighboring oxygen atoms from the surface OH groups and one strong N-H bond of 1.04 Å with the proton on the hematite oxygen atom (see Figure S9). In other

words, ammonia is reacting as a Lewis-base on the bare surface and as a Brønsted-base on the hydrated surface.

The case of the aprotic molecule acetonitrile (**23**) is a structural outlier even though it lies on the diagonal being equally strongly adsorbed on both surfaces (Figure 9). Instead of binding via hydrogen bonds, acetonitrile is sterically so unhindered, that it is able to approach the Fe_{III} site at a 2.15 Å distance, despite the presence of the surface OH bond (see Figure 10). Nevertheless, the interaction of acetonitrile with the surface is among the weakest within the tested library. The same type of adsorption mode on the hydrated surface is also obtained for N,N-dimethylacetamide (**21**) (see Figure S10). However, due to its more significant steric hindrance within the hydration layer, the corresponding adsorption energy is weaker by 0.68 eV on the hydrated compared to the bare surface.

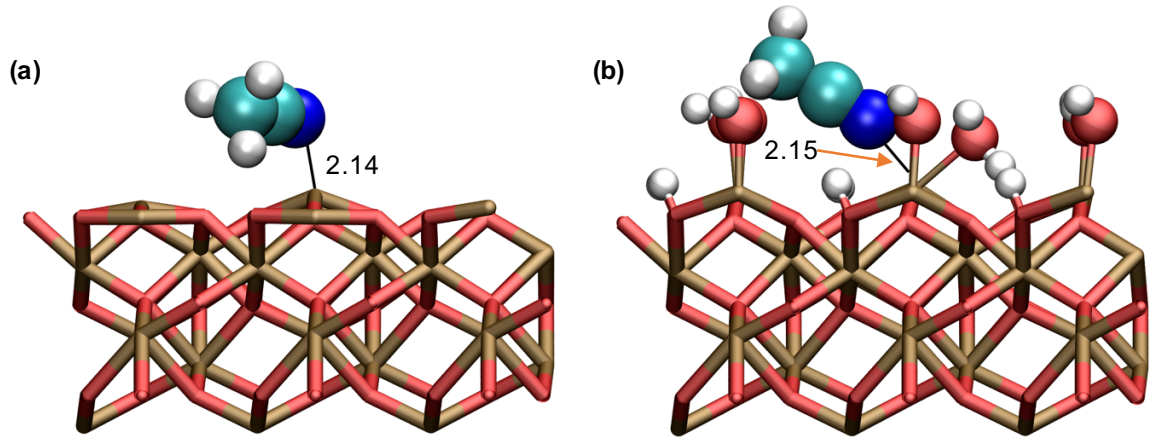

Figure 10: Acetonitrile adsorption on hematite (a) and hydrated hematite (b). Bonds between the molecule and the surface are indicated by continuous lines. Typical bond distances are given in Angstroms.

In close analogy to the situation on alumina, triazole (**9**) is adsorbed with equal strength in the presence and absence of chemisorbed water molecules. Upon triazole adsorption, the hydration layer is reorganized via proton transfers between the hydroxyl groups and the surface protons to maximize the hydrogen bonding (Figure 11). A Fe-N interaction (2.11 Å) is then counter-balancing the loss of a strong interaction with the naked Fe site.

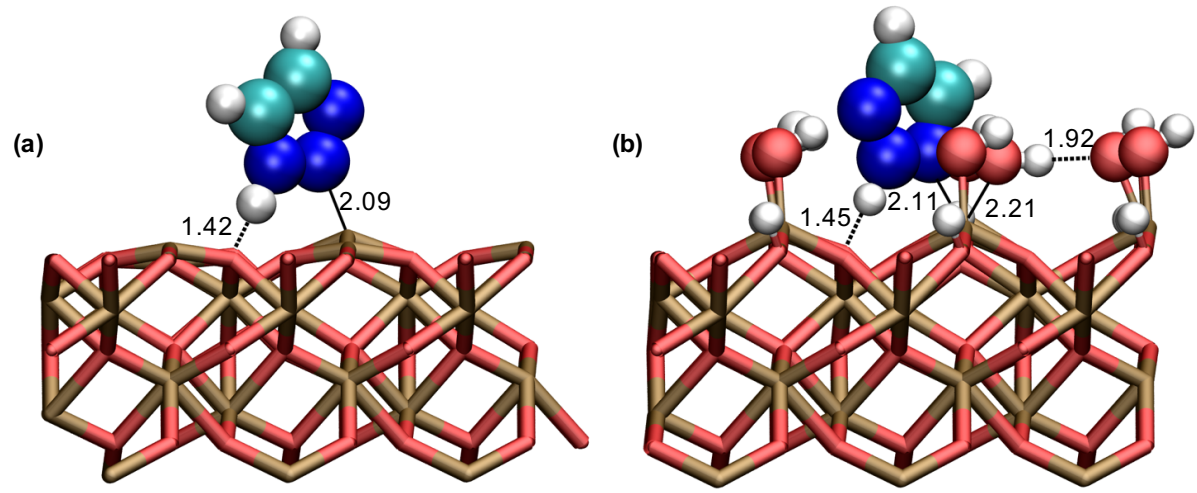

Figure 11: Triazole adsorption on hematite (a) and hydrated hematite (b). Bonds between the molecule and the surface are indicated by continuous lines and hydrogen bonds by dashed lines. Typical bond distances are given in Angstroms.

In summary, since all Lewis-acid sites are occupied by OH groups on the hydrated surface, the adsorption modes of functional groups differ significantly between bare and hydrated hematite. Furthermore, the relative adsorption energies reflect these changes to a certain extent, even though the extrema (most strongly and most weakly adsorbed molecules) remain the same. This is also most clearly seen in Table S2, which summarizes the root mean square deviations (RMSD) over the 25 molecules between various combinations of surfaces to be compared. Indeed, it turns out that adsorption energy on bare hematite differs, on average, more from the one on hydrated hematite than from one on the bare alumina surface. Nevertheless, the deviations are overall small (<0.5 eV), so that estimates of the relative adsorption strength of molecules seem to be transferable from one surface to the others.

3. Towards a fast ranking of additives

The adsorption on alumina of typical functional groups featured by lubrication additives is not very sensitive to the partial hydroxylation (Figure 6). Conversely, ranking found on bare hematite is disturbed by the surface hydration (Figure 9), much more than when moving from bare alumina to bare hematite (Figure 3). Indeed, the full hydroxylation of the Fe sites is disturbing much more the adsorption mode and strength than the partial hydroxylation of alumina. This is attributed to the loss of the strong Fe Lewis acid site. However, adsorption on hydrated alumina and hydrated hematite follow the same trend as illustrated in Figure S11. This is interesting in a screening perspective. Modeling adsorption over hydroxylated hematite is much more expensive than on hydrated alumina due to its anti-ferromagnetic properties and the strong correlation of the 3d electrons. Moving a step

further, we also investigated how the adsorption energy on hydroxylated hematite correlates with the one on dry alumina (Figure S12). The correlation is, with an RMSD of 0.2 eV, (see Table S3), sufficiently accurate that the ranking obtained on the easy to compute dry alumina surface is valuable to predict the ranking on the more realistic hydrated alumina and hydrated hematite.

As a result of our screening, protic molecules are found to be more strongly adsorbed than the aprotic ones. This can be illustrated by the methylphosphate (**5**) vs. the trimethylphosphate (**25**). With two OH groups, the former is clearly the most strongly adsorbed, while the fully methylated phosphate lies in the middle of the ranking. Acidobasic Lewis interaction between the (P)=O and the Lewis sites such as Al or Fe or H-bonding with the surface hydroxyl are not as stabilizing as the dissociation of the PO-H bond. In agreement with our previous screening on bare alumina,[20] the more acidic the protic group is, the stronger is the adsorption. In addition, multidentate head groups are clearly more strongly adsorbed, beneficiating from the accumulation of stabilizing interactions as in N-methyldiethanolamine (**5**) or even triazole (**9**) and succinimide (**11**).

Conclusion

In this paper, we have performed DFT computations to assess the influence of the type of surface and its hydration state on the adsorption of various functional groups, typical for common organic compounds and for polar head groups of lubricant additives. The comparison of the dry alumina and hematite surfaces reveal that adsorbates are, overall, more strongly bound on hematite, indicating that this surface is more reactive. When taking into account the hydration state, i.e., the dissociation of a water molecule on the most reactive Lewis acid site, we have shown that the adsorption energies obtained for hematite and hydrated hematite differ significantly for adsorbates with intermediate adsorption strengths. This can be explained by the fact that water is occupying the only Lewis acid site. Hence, only hydrogen bonds are available abundantly for interactions with adsorbates. Therefore, it is essential to take the hydration state of hematite into account. In the case of the hydrated (100) γ-alumina surface, on the contrary, the water molecule occupies only one out of the four surface aluminum atoms. Therefore, Lewis acid sites are still available for the interactions with adsorbates, leading to a lower adsorption energy difference between the dry and the hydrated surfaces compared to hematite. Moreover, the destabilization induced by the adsorption of the additive on a less acidic adsorption site is at least partially counterbalanced by the formation of stabilizing hydrogen bonds with the surface OH groups. Despite the nominal difference in accessible adsorption sites, hydrated alumina and hydrated hematite are found to give overall the same trends in adsorption energy for the

library of studied functional groups. Finally, even if the adsorption energy values differ from one surface to another, the ranking of the various studied functional groups is largely transferable from one surface model to the other. Thus, once the ranking is obtained for one surface, the results can be used to predict the adsorption on the other surfaces. In particular, the flat, non-magnetic, dry alumina surface is computationally the most convenient model surface allowing a fast screening of additives. Our results are also reassuring from an experimental point of view, as they indicate that model experiments on steel surfaces inform on the performance on aluminum surfaces and vice versa.

Supplementary material

Supplementary materials include side views of the pristine slabs and adsorption structures, tables of the adsorption energies on each surface, complementary data about the comparison analysis and an archive of the adsorption structures in a .xyz format.

Acknowledgments

S. B. gratefully acknowledges Total MS and the ANRT for her PhD fellowship. The authors thank the SYSPROD project and AXELERA Pôle de Compétitivité for financial support (PSMN Data Center) and Nomane Said Omar for his technical support.

Datal Availability

The data that supports the findings of this study are available within the article and its supplementary material.

References

[1] J.D. Kubicki, K.W. Paul, L. Kabalan, Q. Zhu, M.K. Mrozik, M. Aryanpour, A.-M. Pierre-Louis, and D.R. Strongin, Langmuir **28**, 14573 (2012).
[2] R. Réocreux and C. Michel, Current Opinion in Green and Sustainable Chemistry **10**, 51 (2018).
[3] N. Abidi, K.R.G. Lim, Z.W. Seh, and S.N. Steinmann, WIREs Comput Mol Sci (2020).
[4] L.R. Rudnick, editor , *Lubricant Additives: Chemistry and Applications*, 2nd ed (CRC Press, 2009).
[5] M. Saleheen and A. Heyden, ACS Catal. **8**, 2188 (2018).
[6] S.N. Steinmann, P. Sautet, and C. Michel, Phys. Chem. Chem. Phys. **18**, 31850 (2016).
[7] P. Clabaut, B. Schweitzer, A.W. Götz, C. Michel, and S.N. Steinmann, J. Chem. Theory Comput. **16**, 6539 (2020).
[8] C. Michel, J. Zaffran, A.M. Ruppert, J. Matras-Michalska, M. Jędrzejczyk, J. Grams, and P. Sautet, Chem. Commun. **50**, 12450 (2014).
[9] S. Wang, V. Petzold, V. Tripkovic, J. Kleis, J.G. Howalt, E. Skúlason, E.M. Fernández, B. Hvolbæk, G. Jones, A. Toftelund, H. Falsig, M. Björketun, F. Studt, F. Abild-Pedersen, J. Rossmeisl, J.K. Nørskov, and T. Bligaard, Phys. Chem. Chem. Phys. **13**, 20760 (2011).
[10] I.C. Man, H. Su, F. Calle-Vallejo, H.A. Hansen, J.I. Martínez, N.G. Inoglu, J. Kitchin, T.F. Jaramillo, J.K. Nørskov, and J. Rossmeisl, ChemCatChem **3**, 1159 (2011).
[11] F. Calle-Vallejo, D. Loffreda, M.T.M. Koper, and P. Sautet, Nature Chem **7**, 403 (2015).

[12] J. Zaffran, C. Michel, F. Delbecq, and P. Sautet, J. Phys. Chem. C **119**, 12988 (2015).
[13] T.D. Blake and J. De Coninck, Advances in Colloid and Interface Science **96**, 21 (2002).
[14] E. Bertrand, T.D. Blake, and J.D. Coninck, Journal of Physics: Condensed Matter **21**, 464124 (2009).
[15] I. Minami, Applied Sciences **7**, 445 (2017).
[16] J.P. Ewen, D.M. Heyes, and D. Dini, Friction **6**, 349 (2018).
[17] A.G. Merzlikine, L. Li, P.M. Jones, and Y.-T. Hsia, Tribol Lett **18**, 279 (2005).
[18] R.F.G. Apóstolo, G. Tsagkaropoulou, and P.J. Camp, Journal of Molecular Liquids **277**, 606 (2019).
[19] R.A. van Santen and P. Sautet, *Computational Methods in Catalysis and Materials Science: An Introduction for Scientists and Engineers*, 1st ed. (Wiley, 2009).
[20] S. Blanck, S. Loehlé, S.N. Steinmann, and C. Michel, Tribology International **145**, 106140 (2020).
[21] F. Abild-Pedersen, J. Greeley, F. Studt, J. Rossmeisl, T.R. Munter, P.G. Moses, E. Skúlason, T. Bligaard, and J.K. Nørskov, Phys. Rev. Lett. **99**, 016105 (2007).
[22] P. Majumdar and J. Greeley, Phys. Rev. Materials **2**, 045801 (2018).
[23]*Regulation (EC) No 1907/2006 of the European Parliament and of the Council of 18 December 2006 Concerning the Registration, Evaluation, Authorisation and Restriction of Chemicals (REACH), Establishing a European Chemicals Agency, Amending Directive 1999/45/EC and Repealing Council Regulation (EEC) No 793/93 and Commission Regulation (EC) No 1488/94 as Well as Council Directive 76/769/EEC and Commission Directives 91/155/EEC, 93/67/EEC, 93/105/EC and 2000/21/EC (Text with EEA Relevance)* (n.d.).
[24]*Commission Regulation (EU) No 582/2011 of 25 May 2011 Implementing and Amending Regulation (EC) No 595/2009 of the European Parliament and of the Council with Respect to Emissions from Heavy Duty Vehicles (Euro VI) and Amending Annexes I and III to Directive 2007/46/EC of the European Parliament and of the Council (Text with EEA Relevance)* (n.d.).
[25] G.H. Gu, B. Schweitzer, C. Michel, S.N. Steinmann, P. Sautet, and D.G. Vlachos, J. Phys. Chem. C **121**, 21510 (2017).
[26] V. Vorotnikov, S. Wang, and D.G. Vlachos, Ind. Eng. Chem. Res. **53**, 11929 (2014).
[27] M. Salciccioli and D.G. Vlachos, ACS Catal. **1**, 1246 (2011).
[28] R. Réocreux, É. Girel, P. Clabaut, A. Tuel, M. Besson, A. Chaumonnot, A. Cabiac, P. Sautet, and C. Michel, Nat Commun **10**, 3139 (2019).
[29] M. Mishra and D.-M. Chun, Applied Catalysis A: General **498**, 126 (2015).
[30] J. Hutter, M. Iannuzzi, F. Schiffmann, and J. VandeVondele, Wiley Interdisciplinary Reviews: Computational Molecular Science **4**, 15 (2014).
[31] G. Lippert, J. Hutter, and M. Parrinello, Molecular Physics **92**, 477 (1997).
[32] J. VandeVondele, M. Krack, F. Mohamed, M. Parrinello, T. Chassaing, and J. Hutter, Computer Physics Communications **167**, 103 (2005).
[33] S. Goedecker, M. Teter, and J. Hutter, Physical Review B **54**, 1703 (1996).
[34] C. Hartwigsen, S. Goedecker, and J. Hutter, Physical Review B **58**, 3641 (1998).
[35] M. Krack, Theoretical Chemistry Accounts **114**, 145 (2005).
[36] J. VandeVondele and J. Hutter, The Journal of Chemical Physics **127**, 114105 (2007).
[37] J.P. Perdew, K. Burke, and M. Ernzerhof, Physical Review Letters **77**, 3865 (1996).
[38] S. Grimme, J. Antony, S. Ehrlich, and H. Krieg, The Journal of Chemical Physics **132**, 154104 (2010).
[39] S. Grimme, S. Ehrlich, and L. Goerigk, Journal of Computational Chemistry **32**, 1456 (2011).
[40] S. Heiden, D. Usvyat, and P. Saalfrank, The Journal of Physical Chemistry C (2019).
[41] S.K. Ramadugu and S.E. Mason, J. Phys. Chem. C **119**, 18149 (2015).
[42] W.-D. Zabka, T. Musso, M. Mosberger, Z. Novotny, R. Totani, M. Iannuzzi, B. Probst, R. Alberto, and J. Osterwalder, J. Phys. Chem. C **123**, 22250 (2019).
[43] D. Costa, A. Tougerti, F. Tielens, C. Gervais, L. Stievano, and J.F. Lambert, Phys. Chem. Chem. Phys. **10**, 6360 (2008).
[44] K. Corum, A. Abbaspour Tamijani, and S. Mason, Minerals **8**, 91 (2018).
[45] J. An, P. Wanaguru, C. Xia, M. Tao, and Q. Zhang, Physics Letters A **380**, 3149 (2016).
[46] N. Dzade, A. Roldan, and N. de Leeuw, Minerals **4**, 89 (2014).
[47] A. Kotani and T. Yamazaki, Prog. Theor. Phys. Suppl. **108**, 117 (1992).

[48] J. Hubbard, Proc. R. Soc. Lond. A **276**, 238 (1963).
[49] G. Rollmann, A. Rohrbach, P. Entel, and J. Hafner, Phys. Rev. B **69**, 165107 (2004).
[50] X. Huang, S.K. Ramadugu, and S.E. Mason, The Journal of Physical Chemistry C **120**, 4919 (2016).
[51] R.B. Wang and A. Hellman, J. Phys.: Condens. Matter **30**, 275002 (2018).
[52] G.S. Parkinson, Surface Science Reports **71**, 272 (2016).
[53] C. Gattinoni, J.P. Ewen, and D. Dini, J. Phys. Chem. C **122**, 20817 (2018).
[54] M. Blanchard, G. Morin, M. Lazzeri, E. Balan, and I. Dabo, Geochimica et Cosmochimica Acta **86**, 182 (2012).
[55] M.-T. Nguyen, N. Seriani, and R. Gebauer, The Journal of Chemical Physics **138**, 194709 (2013).
[56] J.W. Bennett, X. Huang, Y. Fang, D.M. Cwiertny, V.H. Grassian, and S.E. Mason, J. Phys. Chem. C **123**, 6450 (2019).
[57] B. Gilbert, C. Frandsen, E.R. Maxey, and D.M. Sherman, Phys. Rev. B **79**, 035108 (2009).
[58] R. Réocreux, T. Jiang, M. Iannuzzi, C. Michel, and P. Sautet, ACS Appl. Nano Mater. **1**, 191 (2018).
[59] B.F. Ngouana-Wakou, P. Cornette, M. Corral Valero, D. Costa, and P. Raybaud, The Journal of Physical Chemistry C **121**, 10351 (2017).
[60] M. Digne, P. Sautet, P. Raybaud, P. Euzen, and H. Toulhoat, Journal of Catalysis **211**, 1 (2002).
[61] M. Digne, P. Sautet, P. Raybaud, P. Euzen, and H. Toulhoat, Journal of Catalysis **226**, 54 (2004).
[62] P. Tartaj, M.P. Morales, T. Gonzalez-Carreño, S. Veintemillas-Verdaguer, and C.J. Serna, Adv. Mater. **23**, 5243 (2011).
[63] O. Shekhah, Journal of Catalysis **225**, 56 (2004).
[64] Y. He, F. Guo, K.R. Yang, J.A. Heinlein, S.M. Bamonte, J.J. Fee, S. Hu, S.L. Suib, G.L. Haller, V.S. Batista, and L.D. Pfefferle, J. Am. Chem. Soc. jacs.0c07179 (2020).
[65] J.P. Ewen, C. Gattinoni, N. Morgan, H.A. Spikes, and D. Dini, Langmuir **32**, 4450 (2016).
[66] A. Gouron, K. Le Mapihan, S. Camperos, A. Al Farra, V. Lair, A. Ringuedé, M. Cassir, and B. Diawara, Applied Surface Science **456**, 437 (2018).
[67] S.M.O. Souvi, M. Badawi, J.-F. Paul, S. Cristol, and L. Cantrel, Surface Science **610**, 7 (2013).
[68] M.A. Christiansen, G. Mpourmpakis, and D.G. Vlachos, ACS Catalysis **3**, 1965 (2013).
[69] J. Dawczyk, J. Russo, and H. Spikes, Tribol Lett **67**, 106 (2019).
[70] H. Spikes, Tribology Letters **60**, (2015).
[71] D.A. Sverjensky and N. Sahai, Geochimica et Cosmochimica Acta **62**, 3703 (1998).
[72] N. Sahai and D.A. Sverjensky, Geochimica et Cosmochimica Acta **61**, 2801 (1997).
[73] R.G. Parr and R.G. Pearson, J. Am. Chem. Soc. **105**, 7512 (1983).
[74] R.G. Pearson, J. Am. Chem. Soc. **107**, 6801 (1985).